Supporting Information for "Global estimate of the eddy kinetic energy dissipation from a diagnostic energy balance"

Romain Torres[1], Robin Waldman[1], Julian Mak[2,3], Roland Séférian[1]

[1]CNRM, Université de Toulouse, Météo-France, CNRS, Toulouse, France

[2]Department of Ocean Science, Hong Kong University of Science and Technology, Hong Kong

[3]Center for Ocean Research in Hong Kong and Macau, Hong Kong University of Science and Technology, Hong Kong

Contents of this file

Text S1: Parameterized eddy energy budget in a global ocean model

The NEMO-OMIP2 simulation

The simple eddy energy balance of Equation 3 presented in the main document is first validated within a global ocean model. For this purpose, we use a global OMIP2 hindcast simulation over the period 1958–2018 (Voldoire, 2020). The ocean circulation is solved by NEMO (Nucleus for European Models of the Oceans) version 3.6 (Madec et al., 2017),

———

May 26, 2023, 1:15pm

with the embedded sea ice module GELATO version 6 (Mélia, 2002). An eORCA1 grid is used with a nominal resolution of 1º within the tripolar curvilinear ORCA grid. The model employs 75 vertical levels in z-coordinate and uses the Roquet, Madec, McDougall, and Barker (2015) TEOS-10 approximation for the seawater thermodynamics.

At the air-sea interface, the model is forced at hourly frequency by the Japanese 55-year atmospheric reanalysis for driving ocean models (JRA55-do v1.5.0; Tsujino et al., 2018), using bulk forcing. The experiment is configured in accordance with the 61-year (1958-2018) cycle defined by the OMIP-2 protocol (Tsujino et al., 2020). The simulation was first spun up for three cycles without solving any eddy kinetic energy budget before using the GEOMETRIC parameterization (Mak et al., 2022) for three more cycles. The latter discretizes the EKE budget in Equation 1 and redefines the eddy transport coefficient κ_{gm} accordingly (see the implementation details in the Supporting Information of Mak et al., 2022).

The NEMO-OMIP2 outputs are time-averaged from 1993 to 2017 and then used to analyse the EKE budget. Figure S1 shows the maps for the depth integrated EKE and the associated trends. The dissipation and production terms display similar but opposite patterns confirming the eddy energy balance. In the regions of high EKE horizontal gradients such as the western boundary currents and some spots along the Antarctic Circumpolar Current (ACC), the diffusion term reaches relatively large values even if it is not necessarily the most prominent term. The effect of the advection trend is here particularly minor while the total temporal derivative of EKE is low and contained in highly energetic currents.

Evidence of the eddy energy balance

Using the time-averaged outputs from the NEMO-OMIP2 simulation, the ratio between the baroclinic production and linear dissipation is shown in Figure S2. The energy balance is valid in most part of the ocean area where the ratio "production / dissipation" tend to be close to unity. The diagnostic balance breaks down along the equator, near continental boundaries and locally at mid to high latitudes. These features are mainly explained when analysing the remaining terms of Equation 1 (Figure S1). Along boundaries and at mid to high latitudes, the large levels of energy drive a significant horizontal EKE diffusion which locally breaks the balance. Along the equator, the eddy energy reaches its minimum value leading to a meridional gradient of EKE and thus the diffusion is again non-negligible. However, the largest errors ($> 35\%$) on the eddy energy balance are contained near the coast or at high latitudes, where the EKE is extremely weak.

Method uncertainty quantifications

The computation of the linear eddy kinetic energy dissipation rate λ is based on two main assumptions: 1) the baroclinic production is fully balanced by the linear dissipation and 2) the eddy energy balance can be retrieved from the time averaged ocean stratification. In this section, we detail the method to obtain the uncertainties from these two hypothesis using the NEMO-OMIP2 simulation outputs. However, the modelling choices already described in the main document which result in the formulation of the baroclinic production and the linear dissipation are not discussed.

1. Assuming the eddy energy balance is exact over a given time period leads to the following equality:

$$\overline{P_e} = \lambda \overline{\int \text{EKE} \, dz},\tag{SI-1}$$

where P_e is the baroclinic production saved online by the model and $\overline{}$ denotes for a time averaging operator during the given time period. From this equation, one can compute the dissipation coefficient:

$$\lambda_{\text{bal}} = \frac{\overline{P_e}}{\int \text{EKE} \, dz},\tag{SI-2}$$

Thus, λ_{bal} represents the eddy dissipation rate computed directly from the assumed eddy energy balance and gives the first source of errors when compared to the prescribed *true* λ.

2. The true time averaged production term computed by the model is given by :

$$\overline{P_e} = \alpha \overline{\left(\frac{\int (M^4/N^2) \, dz}{\int (M^2/N) \, dz} \cdot \int \text{EKE} \, dz \right)},\tag{SI-3}$$

However, from an observation-based climatology of ocean temperature and salinity, only the averaged squared horizontal and vertical buoyancy frequencies $\overline{M^2}$ and $\overline{N^2}$ can be computed. We then use the following formulation to estimate errors arising from the time average approximation :

$$\lambda_{\text{av}} = \alpha \frac{\int \left(\overline{M^2}^2 / \overline{N^2} \right) \, dz}{\int \left(\overline{M^2} / \sqrt{\overline{N^2}} \right) \, dz},\tag{SI-4}$$

where $\overline{M^2}$ and $\overline{N^2}$ are also diagnosed online. λ_{av} can then be compared to both λ_{bal} and the prescribed λ to give errors from the time average approximation only and the total (time average + energy balance hypothesis) respectively.

Both errors are mapped in Figure S3. As expected, the eddy energy balance error map is similar in patterns and amplitudes to the ratio between the averaged production and

linear dissipation displayed in Figure S2. In contrast, errors from the time averaging operation show high horizontal dependence with an underestimated λ (negative errors) at lower latitudes and a large overestimation (positive errors) near coastal boundaries. Moreover, errors from the time averaging are low in the Southern Ocean.

The mean relative errors are estimated to 18% for the eddy energy balance and 17% for the time-averaging processing. Combined, a total of 35% error on the eddy dissipation coefficient λ is found, leading to the uncertainty range in our final global EKE dissipation estimate.

As discussed in the main document, this error calculation is based on the model outputs and therefore already includes some biases due to numerical choices in the GEOMETRIC parameterization. Nevertheless, assuming the eddy energy budget and the ocean stratification evolution are to a first order well approximated by the NEMO-OMIP2 simulation, the errors presented here can give an overall idea of the uncertainties for the resulting eddy dissipation rate λ. Since the spatial distribution is model-dependent, an overall metric is needed to be applied in other climatologies and datasets. Thus we computed, two uncertainties for the eddy dissipation rate λ, noted δ_{av} and δ_{bal} using a 68.3% confidence interval (or one standard deviation from the mean):

$$p\left(|\lambda_{\mathrm{av}} - \lambda_{\mathrm{bal}}| < \delta_{\mathrm{av}}\right) = 0.683 \quad \& \quad p\left(|\lambda_{\mathrm{bal}} - \lambda| < \delta_{\mathrm{bal}}\right) = 0.683. \tag{SI-5}$$

where p represents the probability or the percentage of ocean cells where the absolute error is bellow a given level. The Table S1 summarizes the resulting errors and uncertainties from the two identified sources.

Text S2: Computing the vertical structure function $\phi(z)$

May 26, 2023, 1:15pm

The vertical structure fonction is obtained from the World Ocean Atlas 2018 (WOA18) climatology (Garcia et al., 2019) following the method described in LaCasce and Groeskamp (2020); Groeskamp, LaCasce, McDougall, and Rogé (2020). Assuming the mesoscale velocity field is well represented by the linear Quasi-Geostrophic potential vorticity equation and the Brunt-Väisälä frequency N is a function of depth only yields an equation for the vertical structure $\phi(z)$:

$$\frac{d}{dz}\left(\frac{1}{N^2}\frac{d\phi}{dz}\right) + \frac{1}{c}\phi = 0, \tag{SI-6}$$

where c is a surface mode gravity wave phase speed and is initially not known. For the surface boundary condition, a rigid surface is set where the vertical velocity and so $d\phi/dz$ vanishes. By convention, we also fix the condition $\phi(z = 0) = 1$ at the surface. Then a rough bottom boundary condition is considered with zero velocity so that $\phi(z = -H) = 0$. The Equation SI-6 is then solved iteratively from the surface to the bottom using a Runge-Kutta-4 integration method. An initial guess is needed for the gravity wave phase speeds and for that we use:

$$c_{\text{guess}} = \frac{1.5}{\pi}\int_{-H}^{0} N(z)\,dz. \tag{SI-7}$$

Then, a Newton method iterative algorithm is used to adjust the phase speed until the bottom condition with zero velocity is statisfied. The coefficient 1.5 in Equation SI-7 is chosen to improve the convergence. In total, 99.01 % of the profiles converged quickly after 10 iterations. The remaining unconverged profiles are mostly localised at very high

latitudes or close to the coast, and are thus removed when computing the EKE dissipation rate without impacting the results.

Figure S4 shows the e-folding decreasing EKE depth represented by the depth where the squared vertical structure function ϕ^2 equals 0.37. Consistent with Groeskamp et al. (2020), the main patterns are retreived. Notably, low latitudes and shallow waters are home to surface-intensified currents while the Southern Ocean and the Gulf Stream extension area have deeper signatures. However by focusing on the squared vertical function ϕ^2 and the EKE instead of the eddy velocities, our map shows stronger latitude dependance.

References

Garcia, H. E., Boyer, T. P., Baranova, O. K., Locarnini, R. A., Mishonov, A. V., Grodsky, A., ... Zweng, M. M. (2019). World Ocean Atlas 2018: Product documentation. *NOAA National Centers for Environmental Information*. Retrieved from `https://www.ncei.noaa.gov/archive/accession/NCEI-WOA18`

Groeskamp, S., LaCasce, J. H., McDougall, T. J., & Rogé, M. (2020, sep). Full-depth global estimates of ocean mesoscale eddy mixing from observations and theory. *Geophysical Research Letters*, *47*(18). Retrieved from `https://doi.org/10.1029/2020GL089425` doi: 10.1029/2020gl089425

LaCasce, J. H., & Groeskamp, S. (2020, oct). Baroclinic modes over rough bathymetry and the surface deformation radius. *Journal of Physical Oceanography*, *50*(10), 2835–2847. doi: 10.1175/jpo-d-20-0055.1

Madec, G., Bourdallé-Badie, R., Pierre-Antoine Bouttier, Bricaud, C., Bruciaferri, D., Calvert, D., ... Vancoppenolle, M. (2017). NEMO ocean engine. Retrieved from

https://doi.org/10.5281/zenodo.1472492 doi: 10.5281/ZENODO.1472492

Mak, J., Marshall, D. P., Madec, G., & Maddison, J. R. (2022, apr). Acute sensitivity of global ocean circulation and heat content to eddy energy dissipation timescale. *Geophysical Research Letters*, *49*(8). doi: 10.1029/2021GL097259

Mélia, D. S. (2002, jan). A global coupled sea ice–ocean model. *Ocean Modelling*, *4*(2), 137–172. doi: 10.1016/s1463-5003(01)00015-4

Roquet, F., Madec, G., McDougall, T. J., & Barker, P. M. (2015, jun). Accurate polynomial expressions for the density and specific volume of seawater using the TEOS-10 standard. *Ocean Modelling*, *90*, 29–43. doi: http://dx.doi.org/10.1016/j.ocemod.2015.04.002

Tsujino, H., Urakawa, L. S., Griffies, S. M., Danabasoglu, G., Adcroft, A. J., Amaral, A. E., ... Yu, Z. (2020, aug). Evaluation of global ocean–sea-ice model simulations based on the experimental protocols of the ocean model intercomparison project phase 2 (OMIP-2). *Geoscientific Model Development*, *13*(8), 3643–3708. doi: 10.5194/gmd-13-3643-2020

Tsujino, H., Urakawa, S., Nakano, H., Small, R. J., Kim, W. M., Yeager, S. G., ... Yamazaki, D. (2018, oct). JRA-55 based surface dataset for driving ocean–sea-ice models (JRA55-do). *Ocean Modelling*, *130*, 79–139. doi: 10.1016/j.ocemod.2018.07.002

Voldoire, A. (2020). *Cnrm-cerfacs cnrm-cm6-1 model output prepared for cmip6 omip omip2.* Earth System Grid Federation. Retrieved from https://www.wdc-climate.de/ui/cmip6?input=CMIP6.OMIP.CNRM-CERFACS.CNRM-CM6-1.omip2   doi: 10

.22033/ESGF/CMIP6.10345

May 26, 2023, 1:15pm

Table S1.   Eddy dissipation coefficient λ relative errors and uncertainties computed from the

NEMO-OMIP2 simulation outputs. MAE, RMSE and δ stand for the mean absolute error, root

mean squared error and mean bias, respectively.

Error source	MAE	RMSE	δ
Eddy energy balance	0.0018	0.0028	0.0019
Time average	0.0017	0.0026	0.0020
Total	0.0035	0.0046	0.0038
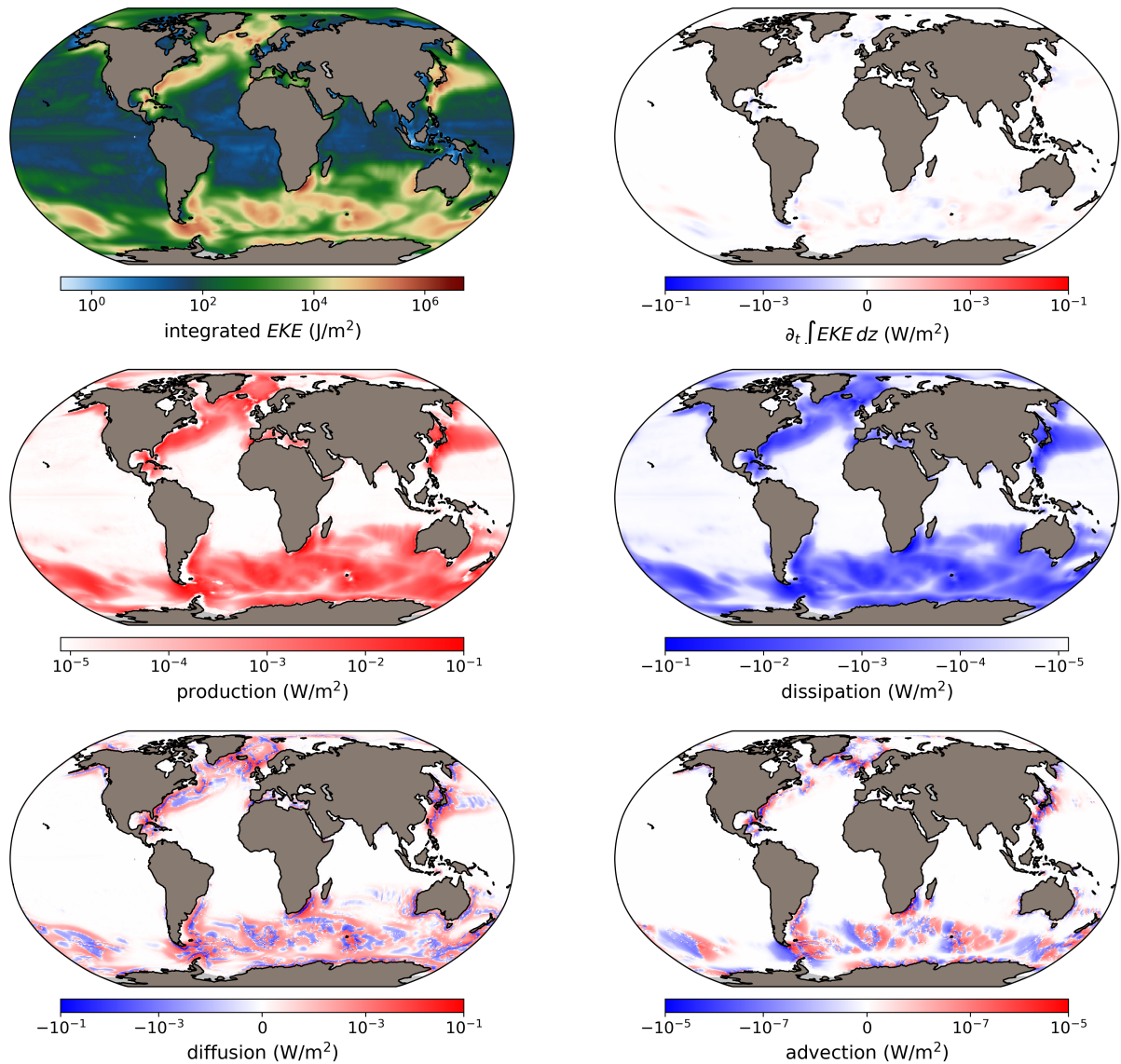
Figure S1. Global maps of eddy energy and the different trends of Equation 1 averaged over the 1995-2017 period of the NEMO-OMIP2 simulation. Since the model uses zero eddy energy background, very weak levels of EKE are found at low latitudes. Colorbars are chosen to be directly comparable except for the advection term which is at least 4 orders of magnitude smaller than other trends. All colorbars also use symmetric logarithmic scales. To convert the units into J and W, a reference density value of $\rho_0 = 1026$ kg/m^3 is used.

May 26, 2023, 1:15pm
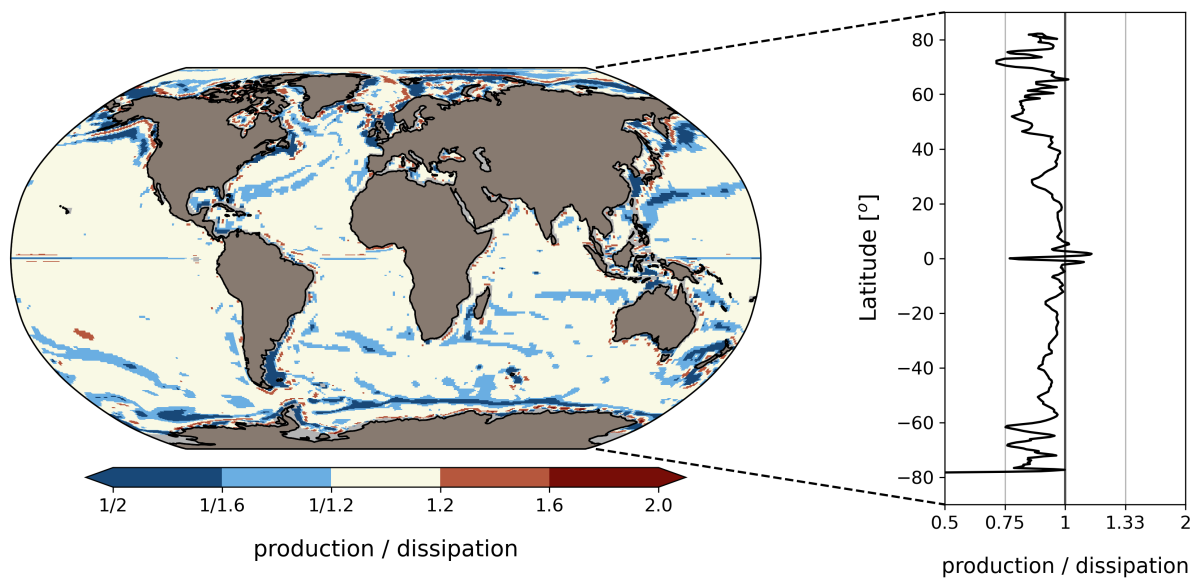
Figure S2. Ratio between baroclinic eddy energy production and linear dissipation in the NEMO-OMIP2 simulation using a parameterized eddy energy budget. Its zonal average is displayed on the right. A geometric scale is chosen for the colorbar to retain proportion both upward and downard unity while a spatial shapiro filter was also used to reduce the horizontal noise.
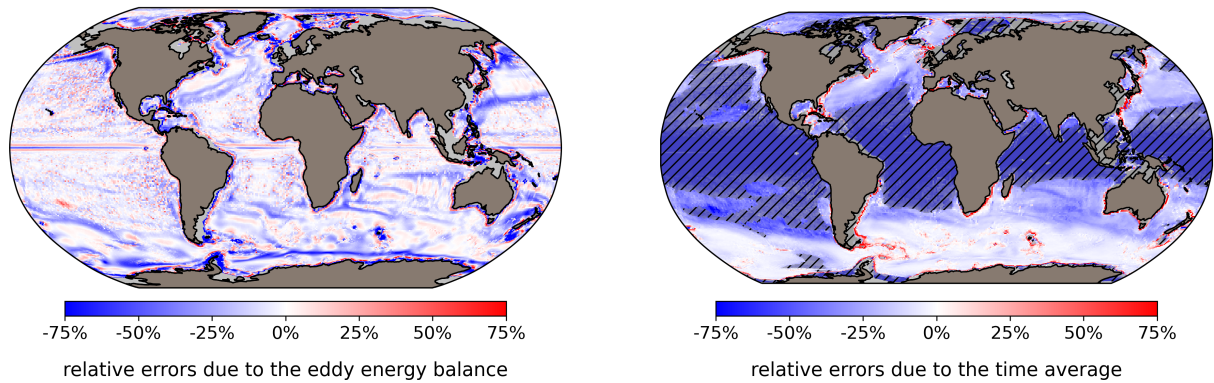
Figure S3. Relative errors due to the eddy energy balance assumption (left) and the time averaging approximation (right) from the NEMO-OMIP2 model outputs averaged from 1995 to 2017. The hatched area covers the ocean cells where the eddy induced transport coefficient κ_{gm} is capped in the GEOMETRIC implementation (see Mak et al. (2022) for details) and therefore the production term is not proportional to the eddy energy. Thus, these cells are not included in the time average error quantification.

May 26, 2023, 1:15pm
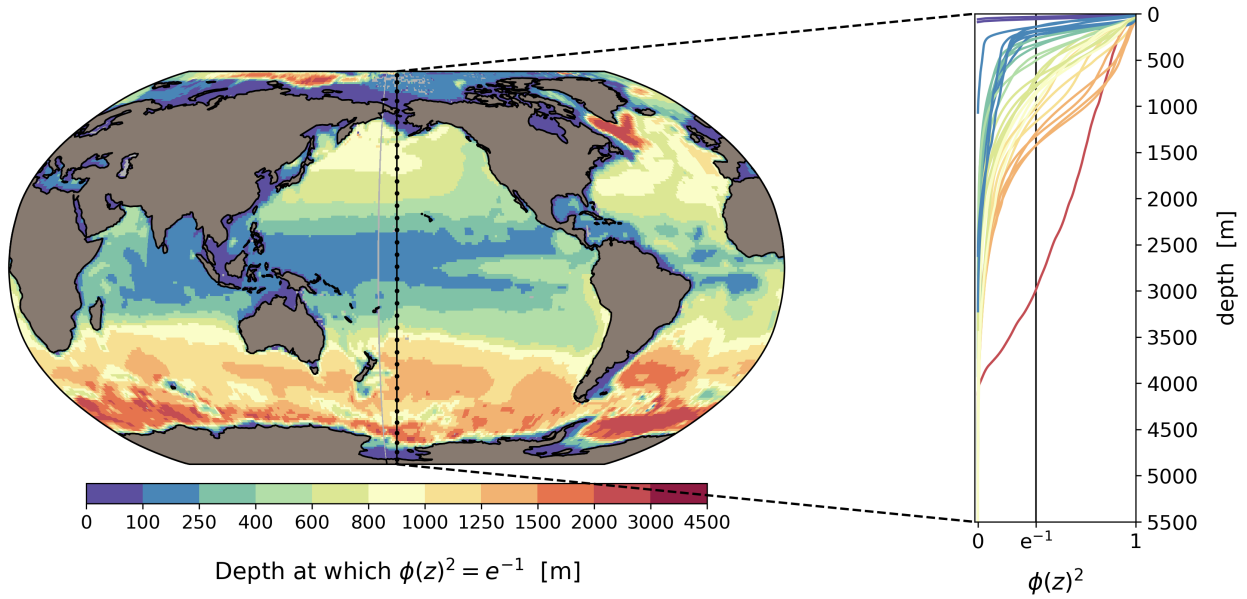
Figure S4. The e-folding depth for the EKE corresponding to the depth where $\phi(z)^2 = e^{-1}$. The map (left) represents the strenght of the EKE decrease with depth while the plot (right) shows profiles along the 171.5°W transect to illustrate the effect of the structure function on the depth integrated EKE.

May 26, 2023, 1:15pm